Supplementary Information

Analytical analysis

According to a previous analytical analysis (Han KH & Frazier AB, 2004, J Appl Phys 96: 5797-5802), the magnetic potential V around a circular ferromagnetic wire (Fig. S1) can be expressed as:

$$V = -r\frac{2\mu_B}{\mu_W + \mu_B}H_0\cos\varphi, \qquad r < a \tag{S1}$$

$$V = -rH_0\cos\varphi + \frac{1}{r}ka^2H_0\cos\varphi, \quad r > a \quad \left(k = \frac{\mu_W - \mu_B}{\mu_W + \mu_B}\right) \tag{S2}$$

where r and φ represent the cylindrical coordinate of the distance and angle, respectively; μ_B and μ_W are the permeabilities of the buffer solution and the ferromagnetic wire, respectively; H_0 is the external magnetic field; and a is the effective radius of the ferromagnetic wire. Then, the magnetic field $\vec{H}_B$ around the wire can be expressed as:

$$\begin{aligned}\vec{H}_B &= -\nabla V = -\frac{\partial V}{\partial r}\vec{a}_r - \frac{1}{r}\frac{\partial V}{\partial\varphi}\vec{a}_\varphi \\ &= \left(H_0\cos\varphi + \frac{1}{r^2}ka^2H_0\cos\varphi\right)\vec{a}_r + \left(-H_0\sin\varphi + \frac{1}{r^2}ka^2H_0\sin\varphi\right)\vec{a}_\varphi, \quad r > a\end{aligned} \tag{S3}$$

where $\vec{H}_B$ represents the magnetic field in the buffer solution around the wire and $\vec{a}_r$ and $\vec{a}_\varphi$ are unit vectors for the *r*- and *φ*-direction in the cylindrical coordinate, respectively.

By substituting $\cos\varphi = \frac{x}{r}$, $\sin\varphi = \frac{z}{r}$ and $r = \sqrt{x^2 + z^2}$ into Eq. (S3), the magnetic field $\vec{H}_B$ can be expressed as:

$$\vec{H}_B = \left[H_0 + \frac{ka^2 H_0 \left(x^2 - z^2\right)}{\left(x^2 + z^2\right)^2} \right] \vec{a}_x + \frac{2xzka^2 H_0}{\left(x^2 + z^2\right)^2} \vec{a}_z , \tag{S4}$$

where x and z represent the Cartesian coordinate and $\vec{a}_x$ and $\vec{a}_z$ are unit vectors for the *x*- and *z*-direction in the Cartesian coordinate, respectively. When $\chi_P \left|\vec{H}_B\right| > M_{PS}$, the magnetic force $\vec{F}_m$ on the beads is:

$$\vec{F}_m = \mu_B V_P M_{PS} \nabla \left|\vec{H}_B\right| , \tag{S5}$$

where χ_p represents the susceptibility of the magnetic beads, V_P is the volume of the magnetic beads, and M_{PS} is the saturation magnetization of the beads. The susceptibility χ_p and the saturation magnetization M_{PS} of the magnetic beads used for analytical and numerical simulations are 0.192 and 30 kA/m, respectively. According to Eq. (S5), the *x*- and *z*-directional magnetic forces (Fig. S2) on a magnetic bead can be rewritten as:

$$F_{mx} = \mu_B V_P M_{PS} \frac{\partial \left| \vec{H}_B \right|}{\partial x}, \text{ and} \tag{S6}$$

$$F_{mz} = \mu_B V_P M_{PS} \frac{\partial \left| \vec{H}_B \right|}{\partial z}. \tag{S7}$$

Then, the *x*- and *z*-directional magnetic forces on a magnetic bead are

$$F_{mx} = -\frac{2V_P M_{PS} xka^2 B_0}{\left(x^2+z^2\right)^2 \sqrt{\left(x^2+z^2\right)^2 + 2ka^2\left(x^2-z^2\right) + k^2a^4}}\left(x^2 - 3z^2 + ka^2\right), \text{ and} \tag{S8}$$

$$F_{mz} = -\frac{2V_P M_{PS} zka^2 B_0}{\left(x^2+z^2\right)^2 \sqrt{\left(x^2+z^2\right)^2 + 2ka^2\left(x^2-z^2\right) + k^2a^4}}\left(3x^2 - z^2 + ka^2\right). \tag{S9}$$

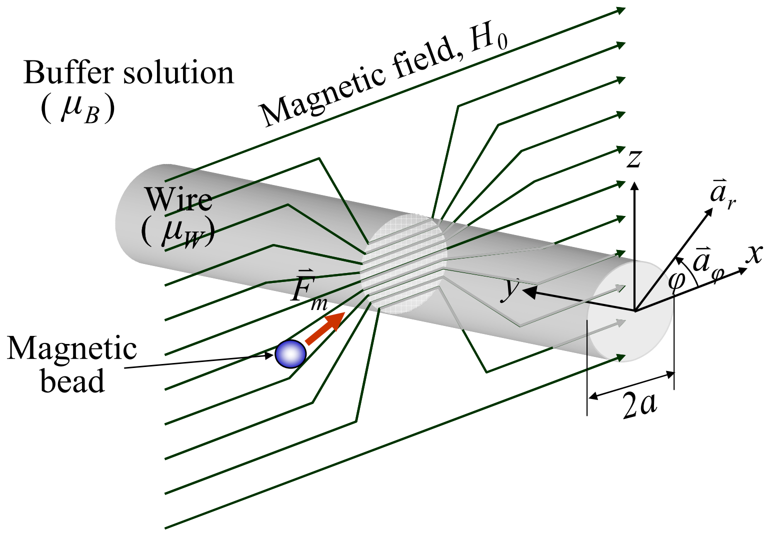

Fig. S1 Cylindrical coordinates of a magnetic bead with respect to a circular ferromagnetic wire in a uniform external magnetic field, H_0.

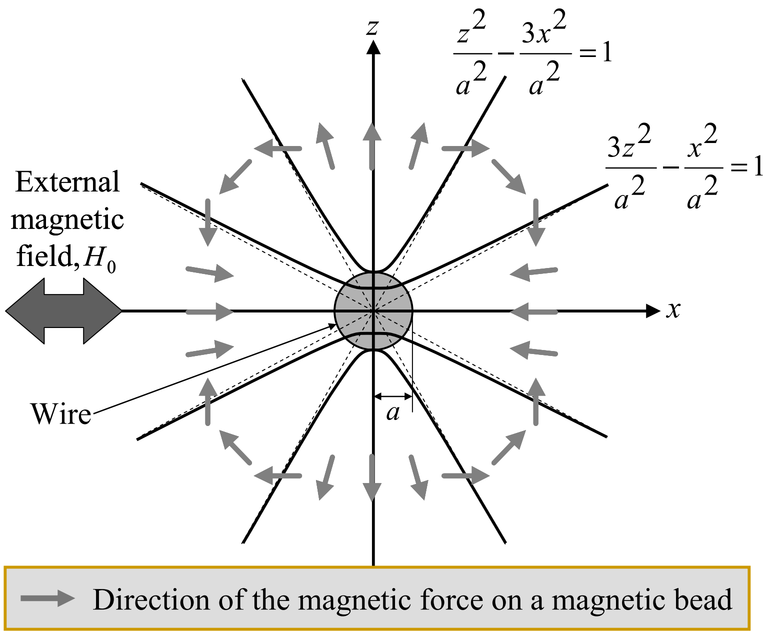

Fig. S2 Direction of the magnetic force on a magnetic bead located around a circular ferromagnetic wire in a uniform external magnetic field, H_0.

Analytical and numerical simulations for the *z*-directional magnetic force

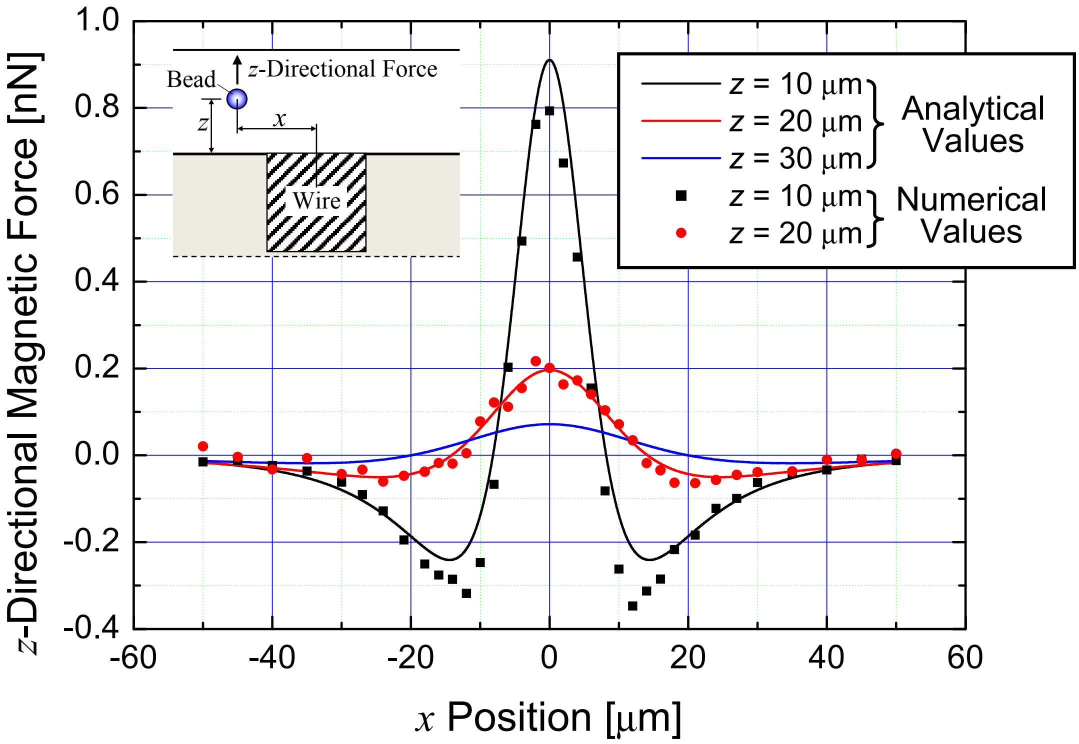

Fig. S3 Analytical and numerical values for the *z*-directional magnetic force for varying levitation heights *z* of a magnetic bead. The hatched square in the inset represents the cross-section of the square ferromagnetic wire, taken perpendicular to the *x*-axis in Figure 1A.

Comparison of the analysis times for a standard RT-PCR method and for the proposed high-speed RT-PCR method

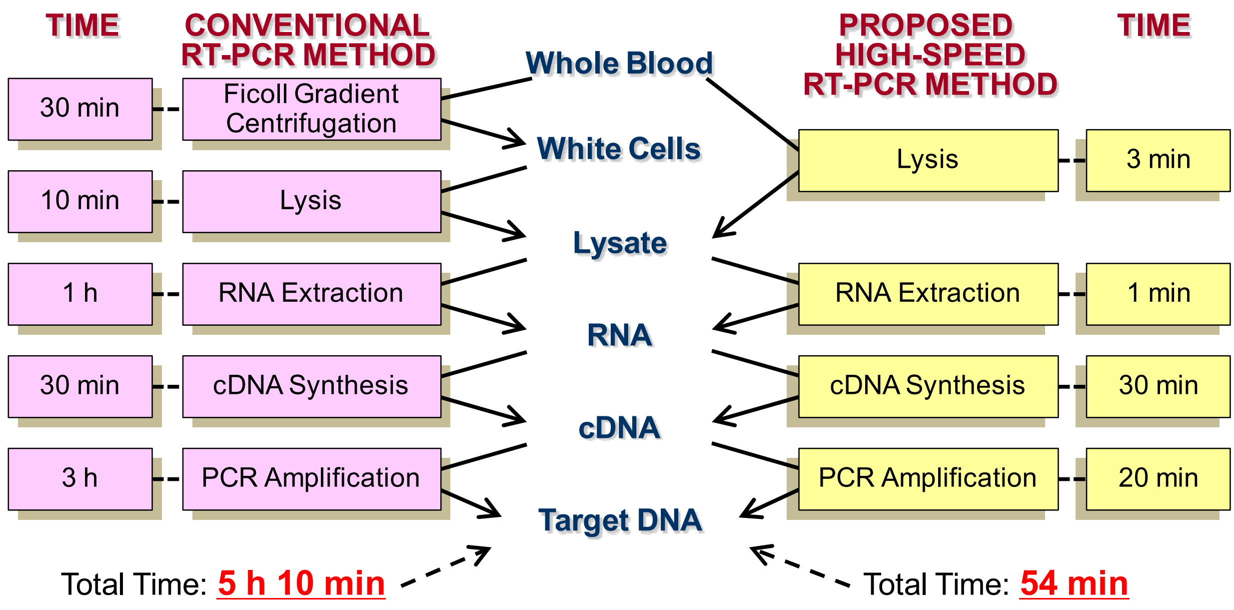

Fig. S4 Process times obtained using a standard RT-PCR method and using the proposed high-speed RT-PCR method for diagnosing blood borne disease. The information on the left of the flow chart provides some general process times for the various methodologies executed with a sample. On the right, we present the process times of the proposed high-speed RT-PCR method.